Journal of Archaeological Science 38 (2011) 1737–1746

Contents lists available at ScienceDirect

Journal of Archaeological Science

journal homepage: http://www.elsevier.com/locate/jas

Measuring use-related fracture velocity in lithic armatures to identify spears, javelins, darts, and arrows

W. Karl Hutchings*

Thompson Rivers University, 900 McGill Road, Kamloops, British Columbia V2C 5N3, Canada

ARTICLE INFO

Article history:
Received 14 November 2010
Received in revised form
23 February 2011
Accepted 4 March 2011

Keywords:
Lithic analysis
Impact fractures
Projectile points
Fracture mechanics
Fracture velocity
Loading rate

ABSTRACT

This study employs a brittle fracture-mechanics-based approach to explore the relationship between lithic fracture velocity and precursory loading rate in fine-grained lithic armatures. The data demonstrate that only high-speed dart and arrow armatures are subject to dynamic loading events, whereas spear and javelin armatures are limited to rapid (and quasi-static) loading. The data presented were derived from controlled experiments employing spears, javelins, spearthrower darts, and arrows. Armatures associated with both bow and spearthrower technologies are reliably identified and distinguished from those of low-speed technologies such as spears and javelins. Javelin armatures may also sustain higher velocity fractures than spear armatures, thus permitting the further differentiation of these technologies. The methodology offers a quantitative, non-subjective means to identify the delivery technology associated with a lithic armature.

1. Introduction

Analysts have long sought an effective method to differentiate lithic projectile and thrusting armatures from other artifacts with similar form, but different use histories. The literature on this issue has identified amply two distinct challenges: 1) identification of criteria that would distinguish a lithic armature (or "point") from other pointed artifacts, and 2) identification of the delivery technology associated with the propulsion of that armature (e.g., Ahler and McMillan, 1975; Barton and Bergman, 1982; Bergman and Newcomer, 1983; Corliss, 1972; Dockall, 1997; Evans, 1957; Fenenga, 1953; Fischer et al., 1984; Forbis, 1962; Frison, 1978; Frison et al., 1976; Holdaway, 1989; Hughes, 1998; Kay, 1996; Lombard and Pargeter, 2008; Marks, 1998; Odell, 1977, 1988; Pargeter, 2007; Roper, 1979; Shea, 1988, 2006; Shea et al., 2001; Shott, 1997; Thomas, 1978; Wadley and Mohapi, 2008; Witthoff, 1968; Woods, 1988; Wyckoff, 1964; Yaroshevich et al., 2010). The term "projectile" is used here in its literal sense to mean an object projected, thrown, or launched forth by force. "Projectile points", therefore, are associated with javelins, spearthrower darts, and arrows. In contrast, a spear is not launched, but is instead a thrusting weapon; spear points, therefore, cannot correctly be referred to as "projectile points".

The narrow tips of pointed implements tend to be fragile, and it is not unreasonable to expect these tips to exhibit damage. Various types of lithic fractures which may otherwise appear identical, however, may result from a wide range of different events and forces, or "loading rates", encountered during manufacture, careless handling, or a variety of use applications. So-called "diagnostic impact-fractures" often observed on pointed implements, for example, are a series of formal tip fractures found on both projectile points and other pointed lithic artifacts and debitage. Even if they were proven "diagnostic" of impact, which is to say that the fracture resulted from sudden contact, there are many different kinds of impact, and not all are related to use. The damage sustained by the tips of high-speed projectile armatures, however, should result from dynamic loading rates and exhibit higher fracture velocities than other artifacts exhibiting morphologically similar damage, but caused by non-projectile-related use. This research presents a novel methodology for the quantitative, non-subjective identification of weapon technologies employing lithic armatures.

2. Definition of loading rate

The term "loading rate" refers herein to the characteristics of contact between two objects including, minimally, the rate of collision, the duration of contact, and the mechanical responses of the materials involved. The concept of loading rate, and its importance, may be explained using an example of a familiar process:

* Tel.: +1 250 371 5767; fax: +1 250 371 5697.
E-mail address: khutchings@tru.ca.

0305-4403/$ – see front matter © 2011 Elsevier Ltd. All rights reserved.
doi:10.1016/j.jas.2011.03.005

During the production of lithic implements, a flintknapper's primary concern is the controlled removal of flakes from a core. This is achieved primarily through manipulation of the loading rate. With respect to percussion flaking, for example, energy is imparted to the core, and controlled by at least five methods: 1) by the selective use of percussors of different densities, 2) by the selective use of percussors of different masses, 3) by the angle of the impact between the percussor and core, 4) by the speed of the impact, and 5) by the support conditions of both the percussor and core. In general fracture mechanics terms, each method is a means of varying the loading rate [modified from Hutchings, 1999: 1437].

A tripartite loading rate scheme modified from Stowe and Ainsworth (1972); see also Tomenchuk (1985); is followed here, and defined for archaeological purposes as follows: quasi-static loading refers to the application of a slowly increasing contact force, and can be roughly equated with the concept of pressure flaking. Rapid loading is achieved by impact, and may be roughly equated with percussion flaking processes (Hutchings, 1999). Dynamic loading is also achieved by impact, but as will be demonstrated here, fractures resulting from dynamic loading are restricted to high-speed armature impacts associated with certain projectile technologies.

To avoid confusion, it is important to understand that this research does not attempt to measure the impact velocity of the weapon armature itself (cf. Odell et al., 1996: 384). Fracture velocity, which is well in excess of the armature impact velocity, is employed primarily as an indicator of precursory loading rate.

3. The effect of loading rate and the determination of fracture velocity

Consider for a moment a, perhaps simplistic, example of a hypothetical impact event involving a high-velocity, stone-tipped projectile, and an animal target. In this example, the initial contact occurs with hair and hide, causing some deceleration of the lithic projectile, but not fracture. Penetration of the target, and deceleration, continues and the projectile's margin contacts a rib at an acute angle causing small multiple fractures along that margin. Continuing on, the projectile decelerates further, until the tip contacts the pelvis on the opposite side of the target; the tip fractures in several places and stops.

During this single hypothetical event, opportunity exists to generate multiple fractures under all three loading rates; rapid loading occurs with rib contact causing multiple fractures along the projectile margin; dynamic loading causes multiple fractures at the contact of the tip and pelvis; and the inertia of the projectile and its haft causes multiple, quasi-static loading events as the broken pieces are pressed into each other until the projectile comes to rest. An analyst examining the fragments of this artifact for evidence of dynamic loading need not be dissuaded by the variety of loading rates, since even a single fracture resulting from dynamic loading constitutes the sought after evidence. Fortunately, very fine-grained brittle solids can preserve a record of the velocity of a fracture. Microscopic ripple marks on the fracture surface can be used to determine the velocity of the fracture, and, subsequently, the precursory loading rate of the impact event. These ripple marks, common on obsidian, may also be observed on less glassy, but still fine-grained materials such as chert, flint, jasper, agate, chalcedony, and ignimbrite.

3.1. Velocity-dependent fracture surface features

Although the terms "crack" and "fracture" may be used synonymously, I attempt to combine fracture mechanics and archaeological conventions, using the term "crack" when discussing phenomena during, and related to, bond rupture; and "fracture" to refer to the product of crack formation. Some synonyms for important fracture mechanics terms are also included in parentheses to assist the reader in avoiding confusion when consulting the technical literature.

Energy imparted to a core is transmitted as a wave-induced stress field, and can initiate a crack if the energy is sufficient to rupture atomic bonds; the crack (fracture) velocity is related to the precursory loading rate. Velocity-dependent fracture surface features are formed by the dynamic interaction of a progressing crack front with two elastic waves, the longitudinal (or dilational) wave, and the distortional (or transverse) wave. These waves are generated by the initial loading event (in the case of the longitudinal wave), and by bond rupture episodes along the crack front (Tomenchuk, 1985: 437–438). The maximum instantaneous fracture velocity (i.e., the fracture velocity at a specified point on the fracture surface) may be determined from the effective angle of divergence of the longitudinal and distortional waves; the relative orientation of these waves may be determined from certain ripple marks expressed on the fracture surface.

Wallner lines (Figs. 1 and 2) are one type of velocity-dependent microscopic ripple mark that may be observed in varying configurations on fracture surfaces. They originate at localized disturbances, such as the fracture boundary, or intrinsic flaws in the stone material, appearing as thin, ripple-like, curvilinear structures that generally become more attenuated with distance from their point of origin. An in-depth review and discussion of Wallner lines and their formation can be found in Tomenchuk (1985).

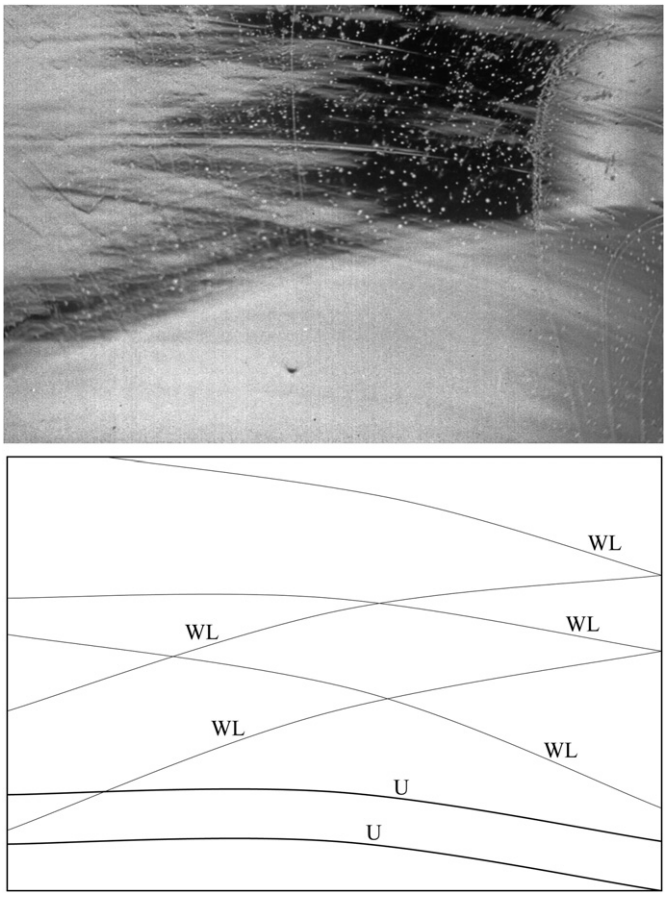

Fig. 1. Photomicrograph of a highly reflective obsidian fracture surface exhibiting fine undulations, and intersecting Wallner lines. Accompanying diagram illustrates locations of pertinent fracture surface features in photomicrograph; Wallner line (WL), undulation (U).

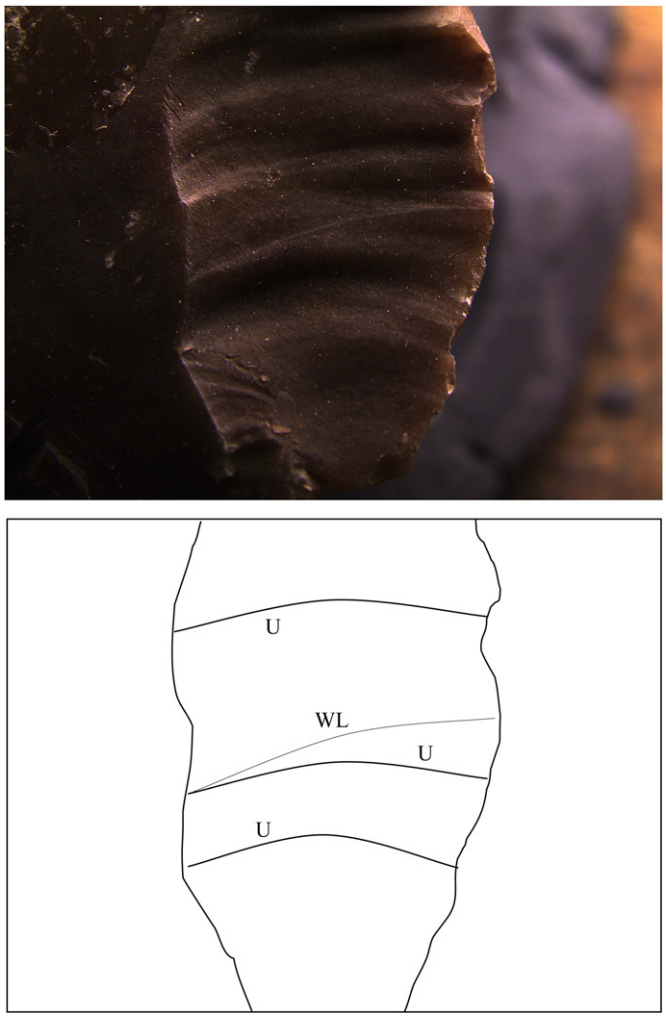

Fig. 2. Photomicrograph of a flint fracture surface exhibiting undulations and a single (oblique) Wallner line originating at the fracture boundary. Accompanying diagram illustrates locations of pertinent fracture surface features in photomicrograph; Wallner line (WL), undulation (U).

Wallner lines are often much finer than, and must not be confused with, fracture undulations; the latter are not velocity-dependent features. Unlike Wallner lines, undulations are concentric about the point of fracture initiation, and vary from macroscopic ripples, often with low-topographic gradients and commonly expressed in exaggerated form near the fracture termination margin of hard-hammer flakes, to narrow, near-microscopic (or even microscopic) ripple marks with comparatively steep topographic gradients (Tomenchuk, 1985: 439). Considered in isolation, the finest undulations may be morphologically indistinguishable from Wallner lines, except that the two will not be formed parallel to one another, but will instead be mutually oblique (Figs. 1 and 2). Most importantly, fracture undulations form parallel along the progressing crack front (i.e., perpendicular to the direction of travel of the longitudinal wave), and as such serve to orient the crack front and, therefore, the longitudinal (or dilational) wave.

Fracture wings are a second type of velocity-dependent microscopic ripple mark that may be observed on fracture surfaces. Originating at intrinsic flaws such as inclusions, and varying in size, they resemble a chevron, or an inverted "V" (Fig. 3), whose apex points towards the location of fracture initiation. Like Wallner lines, to which they are related, the "wings" of the chevron also attenuate with distance, but much more rapidly than those of Wallner lines.

Fig. 3. Photomicrograph of an obsidian fracture surface exhibiting a large fracture wing and numerous smaller fracture wings, on a plane fracture front.

Where present, these fracture surface features are generally observable at low-power magnification, seldom in excess of 40×, using a diffused light source. The instantaneous fracture velocity at the site of a Wallner line or fracture wing is determined from angular measurements derived from the fracture feature itself, or a combination of the fracture feature and the crack front. Photomicrographic records facilitate both ease of measurement and visual documentation for each feature. To minimize measurement errors when recording fracture feature angles, the fracture surface, relative to the optical axis of the microscope, must be mounted as close as possible to perpendicular. Since variations in measurement results are expected due to the experience of the person conducting the assessment, and the limitations of the measuring instrument; whether a protractor reticule, a software-based measurement tool used in association with digital recording, or a common draftsman's protractor used on a printed photograph; multiple assessments of a given angular measure are recommended, and the results averaged, to increase measurement reliability.

3.2. Determination of fracture velocity

Fracture velocity ($\dot{C}$) is expressed as a fraction of the material's distortional wave velocity (C_2). The latter is material dependent, and empirically determined through a dynamic test of stiffness. Expressed as a numerical constant, the distortional wave velocity accounts for differences in the elastic properties of various materials.

Mathematically, the velocity of the distortional wave (C_2) is expressed as (Blitz, 1967: 13; Jaeger and Cook, 1976: 350):

$$C_2 = (G/p)^{1/2},$$

where G is the modulus of rigidity, and p is the material density. The modulus of rigidity (G) is expressed as:

$$G = E/2(1+\nu),$$

where E is Young's modulus, and ν is Poisson's ratio. Young's modulus (E) is expressed as:

$$E = p\nu_s^2,$$

where ν_s is the sonic velocity of the material [modified from Hutchings, 1999: 1439].

It is the material's distortional wave velocity that accounts for differences in the elastic properties of various stone tool materials, and thus permits the valid comparison of fracture velocities and loading rates between materials. Conveniently, values for the elastic properties (i.e., Young's modulus [E], Poisson's ratio [ν], and

the material sonic velocity [v_s]) of many types of stone may be found in the existing mining and engineering literature (e.g., Birch et al., 1942:Table 5-4 for Rugen flint, and Table 5-11 for Modoc and Lipari obsidian); the modulus of rigidity (G) is calculated from the values of the first two properties (i.e., E and ν), plus the material density. Values for the elastic properties, material density, and distortional wave velocity of certain flaked stone tool materials are presented in Table 1.

Various configurations of Wallner lines and fracture wings may be expressed on a fracture surface. The instantaneous fracture velocity ($\dot{C}$) may be determined at the site of one of these features where the orientation of the crack front is also known; from an undulation for example.

The first Wallner line configuration (Fig. 4a) involves a single line originating at a point (S) on the fracture (mirror) boundary. Two angular measurements are taken at any suitable point (P) where the orientation of the crack front can be determined, as, for example, at the intersection of the Wallner line and an undulation (Hutchings, 1999: 1439). The ratio of the fracture velocity ($\dot{C}$) to the distortional wave velocity (C_2) is expressed mathematically as (Kerkhof, 1975: Fig. 14a):

$$\dot{C}/C_2 = \cos\alpha/\cos\beta.$$

The second configuration (Fig. 4b) involves a pair of Wallner lines, one a reflection of the other (see Field, 1971: 9, Fig. 4c), converging on a single point (S_2) at the fracture boundary. The ratio of the fracture velocity ($\dot{C}$) to the distortional wave velocity (C_2) is expressed mathematically as (Cotterell and Kamminga, 1979: 109):

$$\dot{C}/C_2 = \sin\varphi,$$

where the angles (φ) are derived from the tangents to the curves at point (S_2).

The third configuration (Fig. 5a) involves a pair of Wallner lines originating (at points S_1 and S_2) on opposite boundaries of the fracture surface, and intersecting at point P. The ratio of the fracture velocity ($\dot{C}$) to the distortional wave velocity (C_2) is expressed mathematically as:

$$\dot{C}/C_2 = \sin 2\varphi/\left(\cos^2\beta_1 + \cos^2\beta_2 + 2\cos\beta_1\cos\beta_2\cos\varphi\right)^{1/2}.$$

If the intersecting Wallner lines are symmetrical (i.e., $S_1P = S_2P$; Fig. 5b), then the equation reduces to:

$$\dot{C}/C_2 = \sin\varphi/\cos\beta.$$

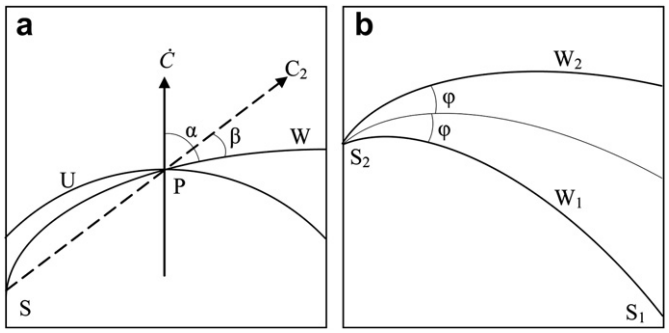

Fig. 4. Variables for the determination of fracture propagation velocity ($\dot{C}$), expressed as a fraction of the distortional wave velocity (C_2), as determined from two discrete configurations of Wallner lines (W). (a) Fracture propagation direction (indicated by $\dot{C}$) is perpendicular to crack front as registered by fracture undulation (U). Distortional wave propagation direction (C_2) indicated by SP, where S is the point of origin of the distortional wave (i.e., the source of disturbance; e.g., fracture boundary), and P is the point of intersection of the generated Wallner line (W) and the fracture undulation (U). (b) Boundary-reflected distortional wave disturbance resulting in the apparent convergence of two Wallner lines (W_1 and W_2; one is a reflection of the other) with mutual angular displacement of 2φ (after Cotterell and Kamminga, 1979:109; Kerkhof, 1975: Fig. 14a; and corrected from Tomenchuk, 1985: Fig. 12.4).

Two configurations of fracture wings may be observed. In the first configuration (Fig. 6a), the fracture front, as well as the fracture wings, are curved. At any points A and A′ where the orientation of the crack front is known (e.g., intersection with an undulation), the angle of divergence is obtained from the intersecting tangents to the fracture wings and the crack front, and is expressed mathematically as:

$$\dot{C}/C_2 = \cos[(\psi/2) - (\delta/2)].$$

In the instance of a plane crack front (i.e., the angle of curvature of the crack front is essentially zero; Fig. 6b), the equation reduces to:

$$\dot{C}/C_2 = \cos\psi/2.$$

Fracture velocities measured at various lengths along the surface of a single fracture indicate that the crack front accelerates rapidly from the point of initiation, reaches maximum velocity at approximately 20–50% of the crack length, and then decelerates towards the termination of the crack. Fracture velocity measurements taken, therefore, between 20% and 50% of the crack length provide the most reliable indication of the precursory loading rate (Hutchings, 1997: 45–46, and Fig. 8; Tomenchuk, 1985:471–472, and Fig. 12.6a). Fortunately, fracture features located this far along

Table 1
Values for the distortional wave velocity of certain flaked stone tool materials. Sources include: (1) Tomenchuk (1985: Table 11.4, and sources cited therein); and (2) Hutchings (1997: Table A1).

Material	p (10^3 N m^{-3})	E [pv_s^2] (10^{10} N m^{-2})	G [$E/2(1+\nu)$] (10^{10} N m^{-2})	ν	C_2 [$(G/p)^{1/2}$] (m s^{-1})	Data source
Chertsey flint (C)	2.52	5.516	2.224	0.24	2971	(1)
Chertsey flint (D)	2.55	5.516	2.224	0.24	2953	(1)
Chertsey flint (E)	2.58	5.516	2.224	0.25	2963	(1)
Rugen flint	2.63	7.45	3.45	0.08	3622	(1)
Edwards (Georgetown) flint	2.63	7.5	3.463	0.08	3629	(2)
Alibates flint (agatized dolomite)	2.62	7.6	3.503	0.08	3664	(2)
Chalcedonic chert	2.56	5.337	2.448	0.09	3092	(1)
Chert (dyke)	2.55	8.274	3.447	0.20	3677	(1)
Dolomitic chert (A)	2.63	3.544	1.648	0.001	2503	(1)
Dolomitic chert (B)	2.67	5.619	2.372	0.14	2981	(1)
Chalcedonic limestone	2.55	4.688	1.875	0.25	2712	(1)
Jaspelite (A)	3.39	10.34	4.826	0.07	3773	(1)
Jaspelite (B)	2.90	7.515	3.916	−0.04	3674	(1)
Modoc Calif. obsidian	2.45	6.56	3.03	0.08	3520	(1)
Lipari obsidian (A)	2.37	6.52	2.78	0.17	3425	(1)
Arnafels Iceland obsidian	2.37	7.18	3.03	0.18	3576	(1)
Glass Butte obsidian	2.546	8.9	3.794	0.17	3865	(2)
Opal	2.34	3.8	1.8	0.06	2774	(1)

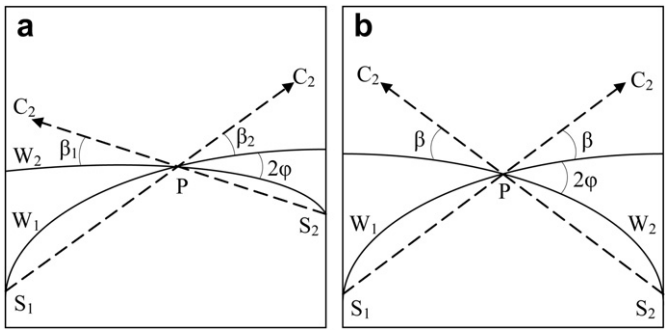

Fig. 5. Variables for the determination of fracture propagation velocity ($\dot{C}$), expressed as a fraction of the distortional wave velocity (C_2), as determined from intersecting Wallner lines (W_1 and W_2). Two distortional wave disturbances (represented by C_2, i.e., S_1P and S_2P) intersect at point P. (a) Asymmetric case. (b) Symmetric case (after Kerkhof, 1975: Fig. 14b–c; Tomenchuk, 1985: Fig. 12.4).

the relatively large fracture surfaces that often result from use-related armature damage are commonly associated with a plane, or near plane, crack front. The result is that the most common fracture feature configuration, fracture wings on a plane crack front (Fig. 3), are easily measured, and, as such, provide an accurate source of fracture velocity data.

4. Dynamic loading of high-velocity projectiles

The expectation that lithic projectile armatures would exhibit fracture velocities in the dynamic range when subjected to high-velocity impacts was investigated, though briefly, during previous research (Hutchings, 1991). Twenty-five velocity-dependent fracture surface features were observed on six damaged, bitruncated rectangular flint microliths from post-Natufian deposits dating to approximately 9000 years ago at Mugharat en-Nachcharini on the Anti-Lebanon Plateau. These microliths, referred to variously as Hagdud Truncations (Bar-Yosef et al., 1987), or Nachcharini Rectangles (Schroeder, 1977), were suspected to have functioned prehistorically, in series with, and proximal to, a microlithic point, as elements of composite projectile armatures. Average $\dot{C}/C_2$ ratios ranging from 0.37 to 0.52, corresponding to average fracture velocities ranging from 1354 m/s to 1873 m/s (instantaneous maxima ranged from 1268 m/s to 2129 m/s) (corrected from Hutchings, 1991: Table 7.15) based on a C_2 value of 3622 m/s for Rugen flint, were obtained from fracture wings exhibited by these artifacts. Subsequently, these fracture velocities compared favorably with those derived from limited experimentation where microlithic flint points and rectangles (a.k.a. truncations) were mounted on 16 arrow shafts as composite armatures, and shot from a hand-held fiberglass recurve bow (11.3 kg draw weight at 750 mm draw length) into meat and bone, and padded leather targets. Average $\dot{C}/C_2$ ratios ranging from 0.33 to 0.50 were derived from 11 fracture wing features on five of the experimental microliths; corresponding average fracture velocities ranged from 1387 m/s to 1498 m/s (instantaneous maxima ranged from 1181 m/s to 1811 m/s) based on a C_2 value of 3622 m/s for Rugen flint (Hutchings, 1991: Table 7.14).

The research indicated that the upper range of fracture velocities associated with dynamic loading would need to be extended beyond Tomenchuk's (1985: Table 12.7) tentative 1500 m/s limit (corresponding to a $\dot{C}/C_2$ ratio of only 0.43) to include fractures resulting from high-velocity impacts (Hutchings, 1991: 212). More importantly, it also suggested that lithic fracture velocity data could be used to identify artifacts used as projectile armatures, and that it may even be possible to distinguish between fracture velocities attributable to specific delivery technologies in a manner similar to that demonstrated by Tomenchuk (1985) for lithic reduction technologies.

4.1. Experimental apparatus

To explore further the implications of those earlier results, a series of controlled experiments were conducted to assess the range of fracture velocities associated with lithic bifacial points used to arm spears, javelins, darts, and arrows. To achieve consistency and repeatability during the experiments, a shooting machine (Fig. 7) capable of launching heavy projectiles at a wide range of velocities was constructed. Resembling a large crossbow with an adjustable draw length, the device was constructed from heavy gauge aluminum, and employed custom-made fiberglass bow limbs with a maximum draw weight of approximately 204 kg. A small boat trailer winch, mounted at the rear of the machine, was used to draw the 2.38 mm diameter, 417 kg test stainless steel bowstring to its locked position in the aluminum trigger mechanism. Projectile velocities were adjusted to match those of specific delivery systems by altering the position of the trigger mechanism, thereby altering the draw length. In some experiments, where lower projectile velocities were required, or lighter projectiles were used, a compound bow with a draw weight of 20.4 kg (at 750 mm draw length) was substituted for the shooting machine, and relative consistency was achieved by marking projectile shafts with the desired draw length necessary to produce a specific velocity.

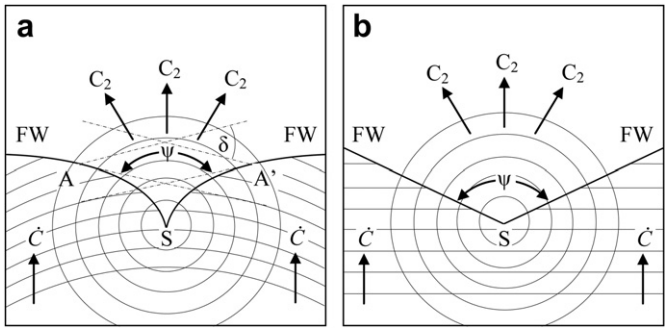

Fig. 6. Variables for the determination of fracture propagation velocity ($\dot{C}$), expressed as a fraction of the distortional wave velocity (C_2), as determined from the effective angle of divergence (ψ) of fracture wings (FW). (a) Circular primary crack front (as indicated by fracture undulation) at point A and A′. The angle of divergence is obtained from the intersecting tangents to the fracture wings at points A and A′. (b) Plane primary crack front. The angle of divergence is measured directly from the fracture wings (after Tomenchuk, 1985: Fig. 12.5; see also Kerkhof, 1975: Fig. 9).

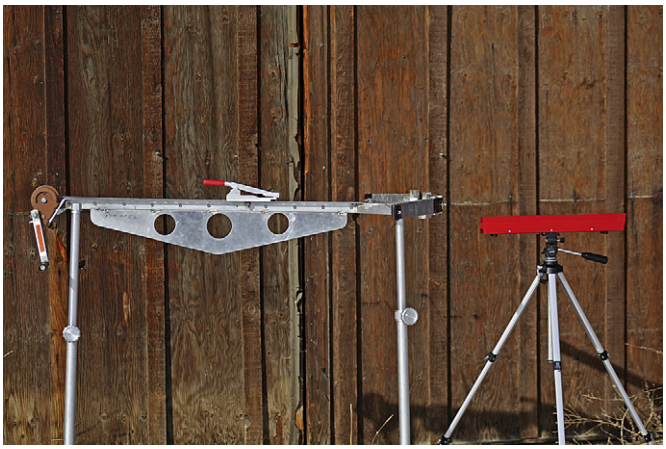

Fig. 7. Ballista-type shooting machine with approximately 204 kg draw weight, and adjustable draw length; custom built for these experiments from aluminum, stainless steel, and fiberglass. The bow limbs have been taped for added safety. A manufacturer-optimized Speedtach, by Custom Chronometer, is at right.

Projectile velocities were measured with a customized archery Speedtach chronometer, manufactured by Custom Chronometer of Sumas, Washington. This photo-electric device was originally designed to measure projectile velocities ranging from those of arrows to small-caliber firearms, and is accurate to approximately 0.3 m/s (1 ft/s). The Speedtach employed was optimized for these experiments by the manufacturer to accurately measure (javelin) velocities as low as approximately 11 m/s (36 ft/s), which are normally below the Speedtach's accurate range.

A brief series of 12 trial shots employing a 230 g dart suggested that shooting machine velocities were consistent to within a range of approximately 1.5 m/s (5 ft/s) at an average velocity of 36.5 m/s (119.7 ft/s). Recorded velocities ranged from 36.0 m/s (118 ft/s) to 37.5 m/s (123 ft/s) (coefficient of variation = 0.01; standard error = 0.41) (cf. Hutchings and Brüchert, 1997). Similar consistency was later observed during the armature fracture velocity experiments. The darts employed were identical to those used in previous experiments by Hutchings and Brüchert (1997); likewise, projectile velocities for the darts were carefully maintained within the limits of the technology as documented by that research (Hutchings and Brüchert, 1997).

4.2. Results of the dynamic loading experiments

The darts and javelins employed in the following series of experiments were also identical to those described by Hutchings and Brüchert (1997), and overall projectile weights and velocities were carefully maintained within the documented limits of each technology. Keeping in mind that the initial requirement of the controlled experiments was to produce broken armatures with observable velocity-dependent fracture features, and that consideration of the distortional wave velocity provided for valid comparisons between different stone materials, a fine-grained Glass Butte (Oregon) obsidian ($C_2 = 3865$ m/s) was selected to maximize the potential for data recovery. In excess of three hundred armatures, replicas of late Pleistocene North American Clovis Paleoindian points, or similarly large, lanceolate, pre-Archaic point types (as defined by Willig, 1989: 13–14) were fashioned by the author for these experiments. Except where otherwise noted, targets for the controlled experiments consisted of several layers of fresh beef ribs supported by straw bale backstops.

4.2.1. Spearthrower darts

Spearthrower darts ranging from 166.7 g to 295.6 g ($\bar{x} = 243.8$ g) were employed for this series of experiments. Projectile velocities averaged 35.6 m/s ($s = 1.44$ m/s; coefficient of variation = 0.04). Kinetic energies ranged from 116.5 J to 165.1 J ($\bar{x} = 147.0$ J). Fracture velocity data recovered from 53 dart armatures produced $\dot{C}/C_2$ ratios ranging from 0.12 to 0.58, indicating fracture velocities spanning the rapid (38%) and dynamic (62%) loading rate ranges (Fig. 8). Summary statistics and distributions are presented in Table 2 and Fig. 9 respectively.

The fact that high-speed projectile impacts do not always produce fractures in the dynamic range indicates that documenting fracture velocity data for a single point may, at times, be insufficient to identify the associated delivery technology. Similar to the hypothetical impact event involving a high-velocity stone-tipped projectile and an animal target described above, the $\dot{C}/C_2$ ratios derived from the dart tests reflect rapid loading rates that actually span the full range of fracture velocities associated with stone tool manufacture. This confirms the notion that the impact fracturing of lithic projectiles is a complex process involving more than just those fractures caused by the extreme force of sudden impact. During these experiments, armatures that penetrated several inches of meat, but failed to contact bone, were rarely damaged. Of course, the beef rib target lacks the hair and hide of a real animal target; without further testing, one may only speculate how this might affect the experimental results, if at all.

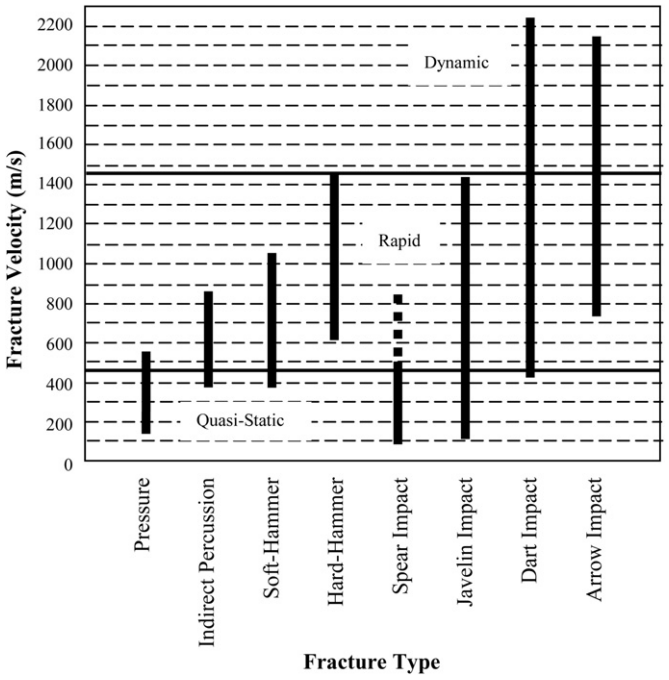

Fig. 8. Comparison of loading rate ranges and experimental lithic fracture velocities associated with various reduction (manufacturing) technologies, and weapon armature impacts. Fracture velocities are based on a C_2 value of 3865 m/s for Glass Butte obsidian.

Of course, darts used for hunting may be expected to miss their targets occasionally. To explore the effect that target density may have on dynamic fracture, a very limited series of tests were made employing a dense stone target rather than softer beef ribs. Six of the darts included in these tests ranged in weight between 274.5 g and 295.6 g, and were shot into a quartzite target by hand using the same spearthrower employed in the dart velocity experiments reported by Hutchings and Brüchert (1997); projectile velocities were not recorded, but are estimated to have ranged between approximately 34 m/s to 43 m/s (cf. Hutchings and Brüchert, 1997: Table 1). A seventh dart, weighing 227.4 g, was shot into a granite target at 35.7 m/s using the shooting machine. In most cases, the lithic armatures were shattered, and the foreshafts severely damaged. Velocity-dependent fracture features were observed on all seven armatures. Interestingly, $\dot{C}/C_2$ ratios for these tests range from 0.27 to 0.54; completely within the normal range of fracture velocities associated with the softer beef rib targets.

While the sample is very small, and lacks the rigor of the controlled experiments, the results are nonetheless consistent with the controlled tests, suggesting that target density may have

Table 2
Basic descriptive statistics for armature fracture velocities ($\dot{C}$).

	Darts	Arrows	Javelins	Spears	Dropped
Sample size	53	15	45	32	15
Minimum	454.28	770.56	101.17	77.57	544.58
Maximum	2230.67	2175.24	1472.84	813.47	1385.09
Average	1561.77	1453.54	922.27	355.16	1076.91
Median	1663.93	1479.07	908.82	357.01	1178.30
Standard deviation	513.75	417.32	329.55	175.24	267.42
Standard error	70.57	107.75	49.13	30.98	69.05
Skewness	−0.57	−0.31	−0.17	0.43	−0.66
Coefficient of variation	0.33	0.29	0.36	0.49	0.25

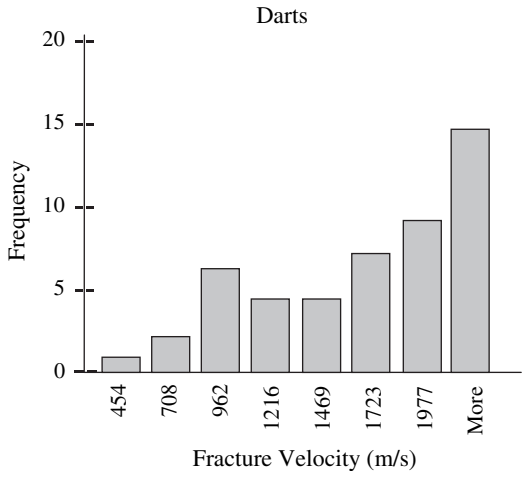

Fig. 9. Frequency distribution of dart armature fracture velocity ($\dot{C}$) data. Note truncation at the upper end of the distribution, and the considerable negative skew.

a much reduced effect on fracture velocity resulting from dynamic loading than was observed for quasi-static and rapid loading during lithic reduction and manufacture. While higher fracture velocities may have been achieved by employing the shooting machine throughout the tests on the stone target, maximum fracture velocities would, regardless, be restricted to the dynamic range, and, theoretically, could not exceed the terminal fracture velocity (i.e., the maximum longitudinal wave transmission rate) of the material; this is approximately 2500 m/s for Glass Butte obsidian (Hutchings, 1997: 58–61), for a $\dot{C}/C_2$ ratio of 0.65.

Naturally, missed shots could also contact less dense materials; dirt or wood for example. Less dense targets, however, could only produce loading rates in one or more of the three defined loading rate ranges, and since it is possible to generate fractures resulting from projectile use that reflect all loading rate ranges, the use of less dense targets would add nothing to the present research.

4.2.2. Javelins

Spears and javelins are distinguished by their mode of use; the former is considered a thrusting weapon while the latter is thrown. Javelins ranging from 137.4 g to 296.4 g ($\bar{x} = 192.7$ g) were employed for this series of experiments. Projectile velocities averaged 25.1 m/s ($s = 0.57$ m/s; coefficient of variation = 0.02). Kinetic energies ranged from 43.3 J to 97.0 J ($\bar{x} = 60.8$ J). Fracture velocity data recovered from 45 armatures produced $\dot{C}/C_2$ ratios ranging from 0.03 to 0.38, indicating fracture velocities spanning the quasi-static (4.4%), rapid (91.2%), and dynamic (4.4%) loading rate ranges (Fig. 8). Notably, only two armatures produced fracture velocities in the dynamic range, both borderline, with $\dot{C}/C_2$ ratios of 0.38. Summary statistics and distributions are presented in Table 2 and Fig. 10 respectively.

As with the dart tests, 10 additional shots were made employing denser targets of granite and quartzite rather than beef ribs. These javelins ranged from 145.8 g to 242.2 g, and were fired under controlled conditions at velocities averaging 24.9 m/s. In most cases, the lithic armatures were shattered, and the foreshafts severely damaged. Velocity-dependent fracture features were observed on nine of the armatures. The $\dot{C}/C_2$ ratios for these tests range from 0.17 to 0.38, which is within the normal range of javelin armature fracture velocities associated with the softer beef rib targets, again suggesting that target density may have a reduced effect on fracture velocities even at the upper range of fractures associated with rapid loading. More importantly, it suggests that regardless of the target, whether intentional or accidental, most lithic fracture velocities for javelin armatures are seldom expected to exceed those of the rapid loading range.

4.2.3. Spears

Spears ranging from 257.7 g to 335.3 g ($\bar{x} = 283.9$ g) were employed for this series of experiments. Spears were thrust manually, with as much force as possible, into beef rib targets. Fracture velocity data recovered from 32 spear armatures produced $\dot{C}/C_2$ ratios ranging from 0.02 to 0.21, indicating fracture velocities spanning the quasi-static (56%) and rapid (44%) loading rates ranges (Fig. 8). None of the spear armatures produced fracture velocities in the dynamic range. In fact, 84% (27 of 32) produced fracture velocities within the (quasi-static) range of those observed for pressure flaking. Summary statistics and distributions are presented in Table 2 and Fig. 11.

My expectations had been that there would be relatively little difference between the fracture velocities associated with spears and javelins, but in retrospect, two important factors offer possible explanations for the results. The first is that javelins benefit from a higher velocity impact resulting from the arm and wrist rotation associated with throwing (Cooper and Glassow, 1968: 122), whereas the velocity of the spear comes mainly from the relatively slow extension of the arm. The second factor may be a direct result

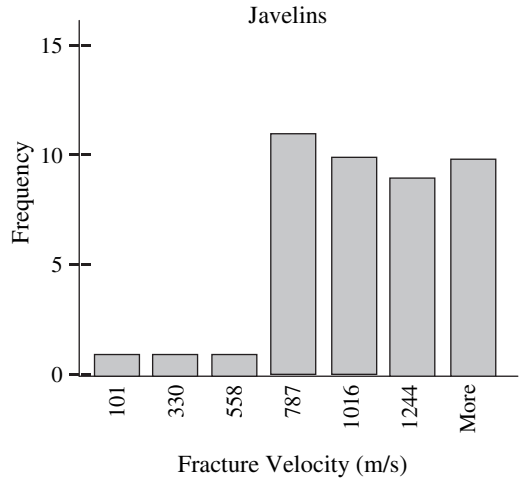

Fig. 10. Frequency distribution of javelin armature fracture velocity ($\dot{C}$) data.

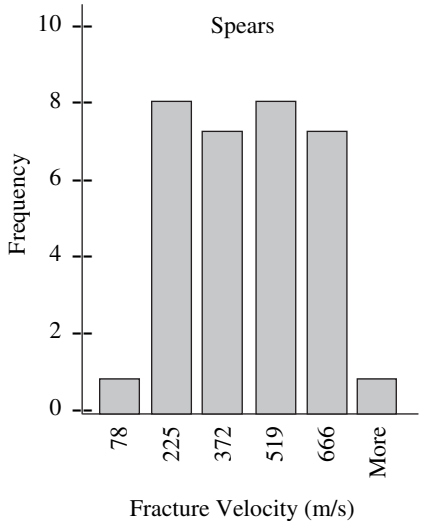

Fig. 11. Frequency distribution of spear armature fracture velocity ($\dot{C}$) data.

of the nature of the loading event itself. Unlike a projectile, which relies on momentum to penetrate a target and is spent after impact, the thrusting action associated with the spear is continuous. The user maintains the thrust through contact with the shaft until the extent of the thrust is reached, or the tip is stopped by contact with bone. The result is continued pressure as the user attempts to complete the thrust. This may explain why most thrusting spear impacts reflect quasi-static loading rates (i.e., resulting in pressure-type fractures), rather than loading rates in the rapid range.

4.2.4. Arrows

Most of the light-weight projectiles employed in the arrow tests consisted of smaller triangular, side- and corner-notched armatures mounted on 9 mm diameter tapered hemlock foreshafts (15 cm in length), connected to 9 mm diameter socketed pine shafts (80 cm in length), others were mounted directly to the pine shafts. Completed arrows ranged from 44.5 g to 55.8 g ($\bar{x} = 49.8$ g) and were fired into beef rib targets with a 20.4 kg (45 lb) draw weight compound bow. Projectile velocities ranged from 33.5 m/s to 46.6 m/s ($\bar{x} = 39.2$ m/s). Kinetic energies ranged from 30.0 J to 48.3 J ($\bar{x} = 38.2$ J). Fracture velocity data recovered from 15 arrow armatures produced $\dot{C}/C_2$ ratios ranging from 0.20 to 0.56, indicating fracture velocities spanning the rapid (46.7%) and dynamic (53.3%) loading rate ranges (Fig. 8). Summary statistics and distributions are presented in Table 2 and Fig. 12.

Interestingly, $\dot{C}/C_2$ ratios derived from the controlled arrow experiments compare quite favorably with those derived from the much smaller and lighter flint microliths described earlier, suggesting that point size, weight, and form, may not be factors that significantly affect loading rate; although insomuch as overall projectile weight (i.e., armature, shaft, adhesive, binding, etc.) affects projectile velocity, overall projectile weight is considered a factor affecting loading rate. Fracture velocity data recovered from the arrow armatures are also quite similar to that of the darts. Considering that kinetic energies for the arrows were less than one third that of the darts and approximately half that of the javelins, one might conclude that impact velocity, rather than kinetic energy, is the essential variable affecting loading rate and fracture velocity in these experiments.

4.2.5. Dropped armatures

It is reasonable to expect that projectile armatures, either hafted or un-hafted, were occasionally subjected to accidental abuse. The most easily damaged portion of a hafted armature might reasonably be its tip and distal lateral margins, and this may result in damage morphologically indistinguishable from intentional use. A series of tests were, therefore, conducted to explore the effects of accidental dropping of armatures onto a hard surface.

All armatures were hafted as spearthrower darts, and dropped from a height of two metres, tip first, onto an andesite boulder. Their velocity upon impact was calculated at 6.3 m/s. Total weights ranged from 225.3 g to 244.6 g ($\bar{x} = 232.1$ g), and their kinetic energies ranged from 4.4 J to 4.8 J. Most damage was in the form of tip fractures; a single armature was shattered, and two suffered burinated lateral margins. Fracture velocity data recovered from 15 armatures produced $\dot{C}/C_2$ ratios ranging from 0.14 to 0.36, indicating fracture velocities within the rapid loading range as expected. Summary statistics and distributions are presented in Table 2 and Fig. 13.

5. Discussion

The results of the fracture velocity experiments indicate clearly that differing delivery technologies expose lithic armatures to different loading rates. Significantly, the controlled experiments demonstrate that the lithic armatures of hand-thrown or thrust weapons incur fractures at rates corresponding to quasi-static and rapid loading, whereas only those lithic armatures propelled at very high speeds, such as those associated with the spearthrower and bow, incur fractures as a result of dynamic loading. The revised correlation of loading rate ranges and associated lithic reduction technologies (Hutchings, 1999) may now be modified to include use-related damage resulting from weapon armature impacts (Table 3). A nonparametric randomization test (Siegel, 1956: 152–158) was conducted to determine the significance of the difference between the sample means of the experimental data. Despite the overlap in instantaneous fracture velocities apparent in Fig. 8, the randomization test demonstrates amply the independence of the samples (Table 4).

The fracturing processes incurred during the impact of a weapon armature are much more complex than those of a single manufacturing type of event. During manufacture, a single blow is carefully controlled and aimed by the knapper to strike the core at a specific location, usually with a very small area of contact. The result is generally a single, well-defined fracture; the intent of the hunter is much different. Weapon armatures are designed to present as much contact area to the target as possible within the limits of the technology. The result of their impact is often a combination of percussion and pressure fractures, initiated at

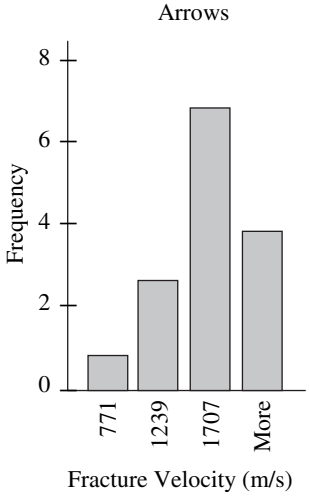

Fig. 12. Frequency distribution of arrow armature fracture velocity ($\dot{C}$) data.

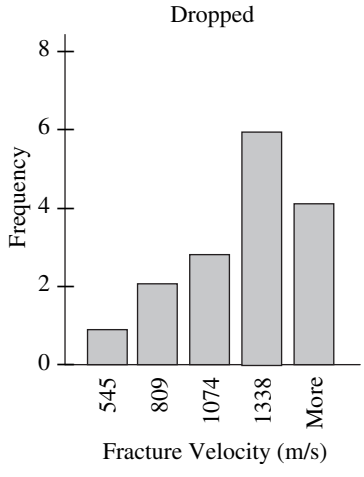

Fig. 13. Frequency distribution of dropped armature fracture velocity ($\dot{C}$) data. Note considerable negative skew.

Table 3
Revised correlation between loading rate ranges, associated lithic reduction technologies or use-damage type, and maximum instantaneous fracture velocities ($\dot{C}$) based on experimental results.

Loading rate ranges	Reduction technology or use-damage	$\dot{C}/C_2$	$\dot{C}$ (m/s)
Quasi-static	Pressure (chest)	0.0–?	0–?
	Spear armature	0.02–0.10	77–385
	Pressure (hand)	0.03–0.10	115–385
	Javelin armature	0.03–0.10	115–385
Rapid	Pressure (chest)	0.10–0.14	385–540
	Spear armature	0.10–0.21	385–812
	Indirect percussion	0.10–0.23	385–890
	Soft-hammer percussion	0.10–0.28	385–1080
	Javelin armature	0.10–0.38	385–1470
	Dart armature	0.12–0.38	420–1470
	Hard-hammer percussion	0.16–0.38	618–1470
	Arrow armature	0.20–0.38	773–1470
Dynamic	Arrow armature	0.38–0.56	1470–2164
	Dart armature	0.38–0.58	1470–2242

Note that maximum instantaneous crack velocities ($\dot{C}$) have been calculated based on a C_2 value for Glass Butte obsidian at 3865 m/s.

various locations around the margins of the armature. Some of these may occur simultaneously, while others may occur in sequence. As a consequence, examination of a single use-damaged armature may be insufficient to identify the delivery technology, since the damage observed may not be the result of an event which accurately reflects the loading rate normally expected for that armature type. For example, experimental point number 69 is an obsidian Clovis lanceolate point replica employed as a dart armature that incurred a large, flute-like tip fracture resulting from impact with bone at 36.3 m/s; experimental point number 163 is also an obsidian Clovis replica, though employed as a javelin armature, that incurred a tip fracture resulting from impact with bone at 25.3 m/s. The tip fractures of both armatures reveal fractures with $\dot{C}/C_2$ ratios of 0.23, indicating fracture velocities of approximately 889 m/s. The data from both fall within the range of fracture velocities observed for soft- and hard-hammer percussion, as well as dart, javelin, and arrow armature impacts, or even accidentally dropped specimens! One cannot reliably assign these fractures to any specific cause based on their known loading rates and fracture velocities, although pressure flaking may be ruled out since their loading rates exceed that known for pressure reduction.

Obviously then, the cause of a specific fracture, based solely on knowledge of the fracture velocity, and, therefore, the precursory loading rate, can only be assigned through exclusion. That is to say, for example, that if a fracture velocity of 1700 m/s were obtained from a given armature constructed from a material with elastic properties similar to Glass Butte obsidian, one may reasonably conclude that: 1) the fracture was not the result of any known manufacturing process, 2) it was caused by a high-velocity impact (i.e., dynamic loading), and, therefore, 3) it was propelled as an arrow or dart armature. Due to its dynamic loading rate, the armature is excluded from any other causes of fracture. Given also, that fracture velocities are a non-subjective, metric determination; a single, reliable measure is all that is necessary for the armature in this example to be confidently assigned to a high-speed impact, such as that expected for an arrow or dart armature.

Table 4
Combined results of the two-tailed randomization test for significant difference between independent samples. Values of p are presented for 10,000 partitions. In all but the darts vs. arrows, and the javelins vs. dropped samples, significant differences are indicated at a confidence level better than 99%.

	Darts	Arrows	Javelins	Spears
Arrows	0.45290	NA		
Javelins	0.00000	0.00000	NA	
Spears	0.00000	0.00000	0.00000	NA
Dropped	0.00120	0.00730	0.10440	0.00000

With respect to the application of this methodology to the archaeological record, it was noted previously that velocity-dependent fracture features are only observable on fine-grained lithic materials (Hutchings, 1999: 1437; and above). Within the study presented, velocity-dependent fracture features were observed on approximately 62% of the replicated obsidian armatures, but this cannot, of course, be considered representative of what may reasonably be expected in the archaeological record since a very fine-grained material was purposely chosen for these experiments, and was used with the intent to produce fractures. Where material selection was possible or practical, lithic materials in the archaeological record will often be biased towards finer grained tool stone. As highly mobile hunter–gatherers, the North American Paleoindians have been noted for purposeful selection of fine-grained lithic materials (Haynes, 1980: 118) and provide some perspective; an examination of 662 Paleoindian artifacts, consisting minimally of various cherts, flints, basalts, obsidians, and quartzites recorded 8.2% that exhibited velocity-dependent fracture features (Hutchings, 1997: 114), though, admittedly, most features were observed on obsidian. For comparison though, Tomenchuk (1985: 454) reports Wallner lines on 10.4% of a sample of 48 English chalk flint blades. While these examples may prove to be best-case scenarios, the quantitative nature of the methodology permits the use of extremely small data sets to demonstrate the presence of a particular technology (cf. Hutchings, 1999); and while there are certainly lithic traditions and industries where this methodology may be difficult, or perhaps even impossible, to employ, it should, nonetheless, prove broadly useful.

6. Conclusions

Our best data are those that are most closely related to the phenomena we are studying; even more desirable, of course, are those data that are *directly* related. To date, in the absence of an intact weapon system, our ability to associate specific weapon armatures with specific delivery systems has been based on the analysis of secondary data derived from patterns that are known to be *associated* with weapon use, but have not been demonstrated satisfactorily to be *exclusive* of other phenomena. In contrast, the methodology presented here (see also Hutchings, 1999) provides data that are not subject to alteration by cultural or natural processes, or open to subjective interpretation. Velocity-dependent fracture features provide a record of dynamic processes governed by universal physical laws; they result directly from the actions that produced them, providing a non-subjective means to assess precursory loading rate.

Since loading rates in the dynamic range are restricted to high-speed impacts associated with bow and spearthrower technologies, lithic armatures associated with these technologies may be reliably identified, and distinguished from javelins and spears; unfortunately, thus far one is still restricted to conventional means to distinguish between dart and arrow armatures, except in technologies that might reasonably be considered much too early for the bow and arrow. The experiments reported here also indicate that some use-damaged javelin armatures will exhibit fracture velocities greater than those possible for spears, and thus these technologies are also distinguishable.

In addition, when considered in combination with previous work (specifically, Hutchings, 1999), this research demonstrates the utility of a quantitative, fracture-mechanics-based methodology for stone tool analysis. While the related fracture mechanics literature

is definitely challenging for the non-specialist, the application of the data collection methodology outlined herein is relatively straightforward:

1) identification and documentation of a relevant fracture surface feature,
2) identification of the specific fracture feature configuration,
3) recording of relevant angular measures, and distance of fracture feature from point of fracture initiation (expressed as a percentage of terminal crack length), and
4) calculation of fracture velocity using appropriate formula for the specific fracture feature configuration.

Of course this assumes that the distortional wave velocity (C_2) of the stone material, or an acceptable comparable material, is known, or values for the material's elastic properties (i.e., Young's modulus [E], and Poisson's ratio [ν]) are available in the existing mining and engineering literature. Where they are not, it is necessary to enlist the services of a specialist in materials engineering to obtain empirical values for these properties. The final variable required for determination of the modulus of rigidity (G), and, finally, the distortional wave velocity (C_2), is the material density (p), which is easily measured as the material's specific gravity, without specialized testing equipment.

Acknowledgements

This research was supported in part by four Simon Fraser University Doctoral Fellowships, and a President's Ph.D. Research Stipend (SFU). Assistance with material testing was provided by Tom Troczynski and Florin Esanu of the Department of Materials Engineering, University of British Columbia. Guidance, comments and suggestions were provided by Roy Carlson (SFU), John D. Speth (U. Mich.), Itamar Kolvin (Hebrew University of Jerusalem), Jack Nance (SFU), David Burley (SFU), and Brian Hayden (SFU); as well as several anonymous peer reviewers.

References

Ahler, S.A., McMillan, R.B., 1975. Material culture at Rodgers shelter: a reflection of past human activities. In: Wood, W.R., McMillan, R.B. (Eds.), Prehistoric Man and his Environments: A Case Study in the Ozark Highland. Academic Press, New York, pp. 163–199.
Barton, R.N.E., Bergman, C.A., 1982. Hunters at Hengistbury: some evidence from experimental archaeology. World Archaeol. 14, 237–248.
Bar-Yosef, O., Gopher, A., Nadel, D., 1987. The "Hagdud Truncation" – a new tool type from the Sultanian Industry at Netiv Hagdud, the Jordan Valley. Mitekufat Haeven 20, 151–157.
Bergman, C.A., Newcomer, M.H., 1983. Flint arrowhead breakage: examples from Ksar Akil, Lebanon. J. Field Archaeol. 10, 238–243.
Birch, F., Schairer, J., Spicer, H., 1942. Handbook of Physical Constants. Geol. Soc. Am., Special Paper 36.
Blitz, J., 1967. Fundamentals of Ultrasonics, second ed. Butterworths, London.
Cooper, J.M., Glassow, R.B., 1968. Kinesiology, second ed. C.V. Mosby, St. Louis (MO).
Corliss, D.W., 1972. Neck width of projectile points: an index of culture continuity and change. Occasional Papers of the Idaho State University Museum 29, Pocatello, Idaho.
Cotterell, B., Kamminga, J., 1979. The mechanics of flaking. In: Hayden, B. (Ed.), Lithic Use-Wear Analysis. Academic Press, New York, pp. 97–112.
Dockall, J.E., 1997. Wear traces and projectile impact: a review of the experimental and archaeological evidence. J. Field Archaeol. 24 (3), 321–331.
Evans, O.F., 1957. Probable uses of stone projectile points. Am. Antiq. 23, 83–84.
Fenenga, F., 1953. The weights of chipped stone points: a clue to their functions. Southwest J. Anthropol. 9, 309–323.
Field, J.E., 1971. Brittle fracture: its study and application. Contemp. Phys. 12, 1–31.
Fischer, A., Hansen, P.V., Rasmussen, P., 1984. Macro and micro wear traces on lithic projectile points: experimental results and prehistoric examples. J. Danish Archaeol. 3, 19–46.
Forbis, R.G., 1962. The Old Woman's Buffalo Jump, Alberta. Contributions to Anthropology, Bulletin 180. Department of Northern Affairs and National Resources, National Museum of Canada, Ottawa.
Frison, G.C., 1978. Prehistoric Hunters of the High Plains. Academic Press, New York.
Frison, G.C., Wilson, M., Wilson, D.J., 1976. Fossil bison and artifacts from an early altithermal period arroyo trap in Wyoming. Am. Antiq. 41, 28–57.
Haynes Jr., C.V., 1980. The Clovis culture. Can. J. Anthropol. 1, 115–121.
Holdaway, S., 1989. Were there hafted projectile points in the Mousterian? J. Field Archaeol. 16, 79–86.
Hutchings, W.K., 1991. The Nachcharini composite projectile: design theory and the study of hunting systems technology at Mugharet En-Nachcharini in the Post-Natufian Levant. M.A. thesis, University of Toronto.
Hutchings, W.K., 1997. The Paleoindian fluted point: dart or spear armature? The identification of Paleoindian delivery technology through analysis of lithic fracture velocity. Ph.D. thesis, Simon Fraser University.
Hutchings, W.K., 1999. Quantification of fracture propagation velocity employing a sample of Clovis channel flakes. J. Archaeol. Sci. 26, 1437–1447.
Hutchings, W.K., Brüchert, L.W., 1997. Spearthrower performance: ethnographic and experimental research. Antiquity 71, 890–897.
Hughes, S.S., 1998. Getting to the point: evolutionary change in prehistoric weaponry. J. Archaeol. Method Theory 5, 345–408.
Jaeger, J.C., Cook, N.G.W., 1976. Fundamentals of Rock Mechanics, second ed. John Wiley & Sons, New York.
Kay, M., 1996. Microwear analysis of some Clovis and experimental chipped stone tools. In: Odell, G.H. (Ed.), Stone Tools: Theoretical Insights into Human Prehistory. Plenum Press, New York, pp. 315–344.
Kerkhof, F., 1975. Bruchmechanische analyse von schadensfällen an gläsern. Glastechnische Berichte 48 (6), 112–124.
Lombard, M., Pargeter, J., 2008. Hunting with Howiesons Poort segments: pilot experimental study and the functional interpretation of archaeological tools. J. Archaeol. Sci. 35, 2523–2531.
Marks, A., 1998. Comment on Plisson et S. Beyries "Pointes ou outils triangulaires? Données fonctionelles dans le Moustérien levantin". Paléorient 24, 18–20.
Odell, G.H., 1977. The application of micro-wear analysis to the lithic component of an entire prehistoric settlement: methods, problems, and functional reconstructions. Ph.D. thesis, Harvard University.
Odell, G.H., 1988. Addressing prehistoric hunting practices through stone tool analysis. Am. Anthropol. 90 (2), 335–356.
Odell, G.H., Hayden, B.D., Johnson, J.K., Kay, M., Morrow, T.A., Nash, S.E., Nassaney, M.S., Rick, J.W., Rondeau, M.F., Rosen, S.A., Shott, M.J., Thacker, P.T., 1996. Some comments on a continuing debate. In: Odell, G.H. (Ed.), Stone Tools: Theoretical Insights into Human Prehistory. Plenum Press, New York, pp. 377–392.
Pargeter, J., 2007. Howiesons Poort segments as hunting weapons: experiments with replicated projectiles. S. Afr. Archaeol. Bull. 62, 147–153.
Roper, D.C., 1979. Breakage patterns of Central Illinois Woodland projectile points. Plains Anthropol. 24, 113–121.
Schroeder, H.B., 1977. Nachcharini, a stratified post-Natufian camp in the Anti-Lebanon mountains. Paper Presented at the 42nd Annual Meeting of the Society for American Archaeology.
Siegel, S., 1956. Nonparametric Statistics for the Behavioral Sciences. McGraw-Hill, New York.
Shea, J.J., 1988. Spear points from the Middle Paleolithic of the Levant. J. Field Archaeol. 15, 441–450.
Shea, J.J., 2006. The origins of lithic projectile point technology: evidence from Africa, the Levant, and Europe. J. Archaeol. Sci. 33, 823–846.
Shea, J., Davis, Z., Brown, K., 2001. Experimental tests of Middle Palaeolithic spear points using a calibrated crossbow. J. Archaeol. Sci. 28, 807–816.
Shott, M.J., 1997. Stones and shafts redux: the metric discrimination of chipped-stone dart and arrow points. Am. Antiq. 62, 86–101.
Stowe, R.L., Ainsworth, D.L., 1972. Effect of rate of loading on strength and Young's modulus of elasticity of rock. In: Gray, K.E. (Ed.), Basic and Applied Rock Mechanics, Proceedings of the Tenth Symposium on Rock Mechanics, University of Texas, May 1968. Society of Mining Engineers, AIME, New York, pp. 3–34.
Thomas, D.H., 1978. Arrowheads and atlatl darts: how the stones got the shaft. Am. Antiq. 43, 461–472.
Tomenchuk, J., 1985. The development of a wholly parametric use-wear methodology and its application to two selected samples of Epipaleolithic chipped stone tools from Hayonim Cave, Israel. Ph.D thesis, University of Toronto.
Wadley, L., Mohapi, M., 2008. A segment is not a monolith: evidence from the Howiesons Poort of Sibudu, South Africa. J. Archaeol. Sci. 35, 2594–2605.
Willig, J.A., 1989. Paleo-Archaic broad spectrum adaptations at the Pleistocene–Holocene boundary in Far Western North America. Ph.D. thesis, University of Oregon.
Witthoff, J., 1968. Flint arrowpoints from the Eskimo of Northwestern Alaska. Expedition 10, 30–37.
Woods, J.C., 1988. Projectile point fracture patterns and inferences about tool function. Ida. Archaeol. 11, 3–8.
Wyckoff, D.G., 1964. The Cultural Sequence of the Packard Site, Mayes County, Oklahoma. Archaeological Site Report, No. 2, Oklahoma River Basin Survey Project. University of Oklahoma Research Institute, Norman.
Yaroshevich, A., Kaufman, D., Nuzhnyy, D., Bar-Yosef, O., Weinstein-Evron, M., 2010. Design and performance of microlith implemented projectiles during the Middle and Late Epipalaeolithic of the Levant: experimental and archaeological evidence. J. Archaeol. Sci. 37, 368–388.